

Combinatorial Approach to the Development of a Single Mass $\text{YVO}_4:\text{Bi}^{3+},\text{Eu}^{3+}$ Phosphor with Red and Green Dual Colors for High Color Rendering White Light-Emitting Diodes

Lei Chen,^{†,‡} Kuo-Ju Chen,[§] Chun-Che Lin,[†] Cheng-I Chu,[†] Shu-Fen Hu,^{||}
Min-Hung Lee,[§] and Ru-Shi Liu^{*,†}

Department of Chemistry, National Taiwan University, Taipei 106, Taiwan, School of Materials Science and Engineering, Hefei University of Technology, Hefei 230009, China, Institute of Electro-optical Science and Technology and Department of Physics, National Taiwan Normal University, Taipei 116, Taiwan

Received April 14, 2010

Instead of developing a novel red phosphor individually, this work proposes the production of white light by combining a near-ultraviolet/ultraviolet diode chip with blue and special yellow phosphors: the yellow phosphor includes the red and green components with high color saturation. The availability of this scheme is demonstrated by preparing a white light-emitting diode (WLED) with color rendering index (Ra) up to 90.3. The desired single-mass yellow phosphor is successfully screened out from the $\text{YVO}_4:\text{Bi}^{3+},\text{Eu}^{3+}$ system by using a combinatorial chemistry approach. When the emission color and luminous efficiency are both considered, the best composition for producing white light is $(\text{Y}_{1-s-t}\text{Bi}_s\text{Eu}_t)\text{VO}_4$ with $0.040 \leq s \leq 0.050$ and $0 < t \leq 0.015$. The red component that is required for a high-Ra WLED is obtained through sensitizing luminescence of Eu^{3+} by Bi^{3+} in a YVO_4 host; meanwhile, both Bi^{3+} and Eu^{3+} emission are improved by keeping the Bi^{3+} and Eu^{3+} contents close to the critical concentration.

Introduction

White light-emitting diodes (WLED) have attracted considerable attention owing to their long lifetime, low energy consumption, low-voltage power requirement, environmental friendliness, and high reliability. They have great potential to replace conventional incandescent and fluorescent lamps.^{1–4} The progress made in the field of LEDs is surprising. For example, the luminescence efficiency has been improved from nearly 60 lm/W in 2005 to 150 lm/W in 2009⁵ (Nichia⁶ reported 249 lm/W for a white LED at 20 mA experimentally). Their range of applications has been extended from voltage signal indicators, initially, to liquid crystal display (LCD) panels backlight for mobile phones and TV sets, automobile lights, traffic lights, street lighting, and outdoor decoration, among others, but obstacles to their use are considerable. Most commercially available WLEDs are produced by combining a blue diode chip with $\text{Y}_3\text{Al}_5\text{O}_{12}:\text{Ce}^{3+}$ (YAG: Ce^{3+}) phosphor, which exhibits yellow luminescence. The main disadvantages of YAG-based WLEDs are their poor color rendering and the severe thermal quenching of the luminescence. The color rendering index (Ra) of the YAG-based LED is about 80, which suffices for general illumination.⁴ However, it is not suitable for certain

medical applications or architectural lighting (such as, museums, libraries, and clothing or cosmetic sales stores), because of the poor performance in the red part of the spectrum.⁴ Accordingly, the production of white light by combination of red, green, and blue phosphors with a near-ultraviolet/ultraviolet (NUV/UV) GaInN diode is highly favored. LED manufacturers globally want to develop them in view of the huge potential market in home lighting. Faced with this trend, the diode chip with short-wavelength emission from 460 nm (blue) through 380–400 nm (NUV) to 325–350 nm (deep ultraviolet) and a shortest extreme ultraviolet emission of 210 nm was a breakthrough quickly.^{7,8} Correspondingly, new highly efficient red, green, and blue phosphors must be developed rapidly so as to keep up with the advances made in diode emission wavelength.

A combinatorial chemistry approach, characterized by parallel synthesis and high through-put screening, has potential to accelerate the development of new phosphors for LEDs.^{9–11} Even some intelligent algorithms, such as Genetic, Monte Carlo techniques, Simulated Annealing, and Artificial Neural Networks algorithms, can be used to speed up lead discovery and optimization and improve the probability of the discovery of objective compounds.^{12–17} Recently, Sohn et al has used a genetic algorithm, which is a systematic approach based on a global optimization strategy through imitating the evolutionary process with elitism, selection, crossover, and mutation operations randomly, in combinatorial approach to optimize novel phosphors for light-emitting diodes.^{9,10}

* To whom correspondence should be addressed. E-mail: rslu@ntu.edu.tw.

[†] National Taiwan University.

[‡] Hefei University of Technology.

[§] Institute of Electro-optical Science and Technology, National Taiwan Normal University.

^{||} Department of Physics, National Taiwan Normal University.

Although some good candidates for green and blue phosphors have been developed for NUV/UV tricolor WLEDs, promising red phosphors have not yet been found.^{10,18} Hence, the development of a good red phosphor is critical to NUV/UV WLEDs. Alternatively, white light with high Ra can be produced by mixing blue with a special yellow that comprises red and green with high color saturation. A plant growth lamp utilizing a NUV light-emitting diode chip and $A_3MgSi_2O_8:Eu^{2+},Mn^{2+}$ ($A = Ca, Sr, Ba$) (AMS-EM) phosphor with emission spectra consisting of blue and red bands has been reported, which is through tailoring the cations composition of AMS-EM in accordance with the change of energy transfer from Eu^{2+} to Mn^{2+} in the host lattice to adjust light quality of the lamp.^{19,20} On the other side, strong green emission from Bi^{3+} was observed in YVO_4 host under NUV excitation,²¹ and several investigations of Eu^{3+} luminescence sensitized by Bi^{3+} in YVO_4 host have been published including for the purpose of solid state lighting applications.^{21–25} However, no work has yet exploited monochromatic green light emitted from Bi^{3+} and red light emitted from Eu^{3+} simultaneously to produce polychromatic yellow light. In this study, a special dual-color phosphor of $YVO_4:Bi^{3+},Eu^{3+}$, which is very suitable for fabricating high-Ra NUV/UV WLEDs for containing a red component from Eu^{3+} emission, was optimized by using a combinatorial chemistry approach; and a WLED has been prepared from the optimized phosphor and a commercially available blue phosphor, with Ra of up to 90.3.

Experimental Section

Combinatorial libraries were synthesized by inkjetting precursor solutions into microreactors using a homemade inkjet delivery system in the sequence $V \rightarrow Y \rightarrow Bi \rightarrow Eu \rightarrow V \rightarrow Y \rightarrow Bi \rightarrow Eu$. The details of the inkjet instrument can be found in our earlier report.²⁶ The precursor solutions were prepared by dissolving appropriate amounts of $Y(NO_3)_3 \cdot 6(H_2O)$ (99.9%), NH_4VO_3 (98%), $Eu(NO_3)_3 \cdot 5H_2O$ (99.99%), and Bi (99.5%) in deionized water. NH_4VO_3 solution was prepared by adding an appropriate amount of NH_4OH to deionized water and heating to 70–80 °C to accelerate dissolution. The Bi^{3+} solution was prepared by adding an appropriate amount of nitric acid to deionized water before the Bi was added, and heating to 70–80 °C to accelerate dissolution. After drying at 60–70 °C, the microreactors that contained precursors were presintered at 600 °C for 3 h, and then sintered at 1100 °C for 3 h to yield the final combinatorial library.

The overall luminescence of the combinatorial library of samples was characterized with a photography method using a digital camera. The emission spectrum of each sample in the library was obtained using a combinatorial scanning fluorescence characterization system. The details of the equipment can be found elsewhere,²⁷ which mainly comprises an Hg lamp, a portable optical fiber spectrometer (Ocean Optics, Inc., model SD2000), and an x-y stage. The materials library was fixed on the x-y stage. Emission spectra from the materials in each microreactor were measured when the fiber-optic probe was focused on the bottom of the

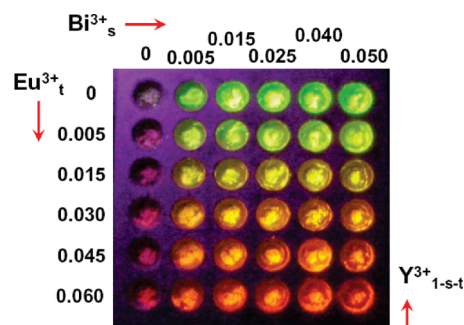


Figure 1. Composition map of the $(Y_{1-s-t}Bi_sEu_t)VO_4$ combinatorial library and its luminescent photograph under 365 nm excitation.

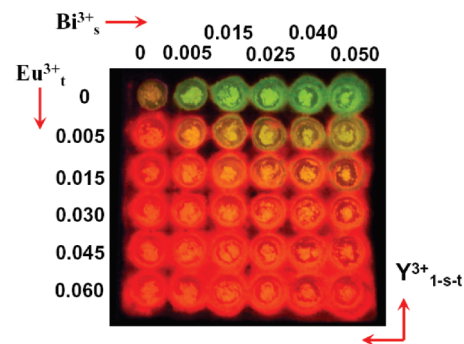


Figure 2. Composition map of the $(Y_{1-s-t}Bi_sEu_t)VO_4$ combinatorial library and its luminescent photograph under 254 nm excitation.

reactor. A light shield was used to prevent interference from other samples.

Results and Discussion

Combinatorial Experiments Results. Figure 1 shows the composition map of the $Y_{1-s-t}VO_4:Bi^{3+}_s, Eu^{3+}_t$ combinatorial library and luminescent photograph under 365 nm excitation. The first column in Figure 1, without Bi^{3+} co-doping ($s = 0$), clearly reveals that the faint red emission of Eu^{3+} increases with Eu^{3+} concentration from $t = 0$ to $t = 0.060$, even though the emission of Eu^{3+} is very weak. The other columns ($s = 0.005, 0.015, 0.025, 0.040,$ and 0.050 , respectively) demonstrate bright luminescence is observed, and the emission color changes from green to orange as the Eu^{3+} concentration increases from $t = 0.005$ to $t = 0.060$. The first row in Figure 1, without Eu^{3+} co-doping ($t = 0$), clearly shows that the strong green emission of Bi^{3+} increases with Bi^{3+} concentration from $s = 0$ to $s = 0.050$, and this increase is not obvious when Bi^{3+} content exceeds $s = 0.025$. The other rows ($t = 0.005, 0.015, 0.030, 0.045,$ and 0.060 , respectively) indicate that the emission color almost does not change, but the brightness increases with Bi^{3+} concentration from $s = 0.005$ to $s = 0.040$, and then declines as Bi^{3+} concentration increases further. When $t = 0.015–0.060$, the brightness is greatly reduced at $s = 0.050$. These phenomena suggest that Eu^{3+} can not emit efficiently without Bi^{3+} co-doping under 365 nm excitation, but that excessive Eu^{3+} co-doping seriously quenches Bi^{3+} luminescence.

Figure 2 displays the luminescent photograph of the $(Y_{1-s-t}Bi_sEu_t)VO_4$ combinatorial library under 254 nm excitation. A comparison with Figure 1 clearly reveals a significant difference between 365 and 254 nm excitation, and thereby, the special role of Bi^{3+} in luminescence. When

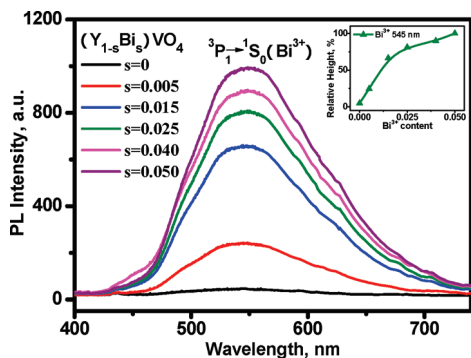


Figure 3. Emission spectra of samples with $s = 0–0.050$ and $t = 0$ in the $(\text{Y}_{1-s}\text{Bi}_s)\text{VO}_4$ combinatorial library under 365 nm excitation.

the Bi^{3+} content is zero, strong emission from Eu^{3+} is observed in Figure 2. The emission increases with Eu^{3+} concentration from $t = 0$ to $t = 0.045$. Even though green emission from Bi^{3+} is also observed at 254 nm excitation, the red emission from Eu^{3+} dominates when the Eu^{3+} concentration is not less than the Bi^{3+} concentration. When a diagonal line is drawn from the top left to the bottom right, the bottom left area is brighter than the top right area. The YVO_4 host can absorb an excitation wavelength of 254 nm and transfer the energy efficiently to the Eu^{3+} activators. However, this process is not efficient with excitation at 365 nm.^{21,25} The significant difference of luminescence between 365 and 254 nm excitation reveals that co-doping Bi^{3+} in $\text{YVO}_4:\text{Eu}^{3+}$ increases its suitability for use in NUV WLEDs because doped Bi^{3+} ions promote the red-shift of the absorption band from UV to NUV.

To analyze spectral composition and luminous efficiency, the emission spectra of every sample in the $(\text{Y}_{1-s-t}\text{Bi}_s\text{Eu}_t)\text{VO}_4$ combinatorial library were obtained. Figure 3 presents the emission spectra of the samples in the first row with $t = 0$ and $s = 0–0.050$ in the combinatorial library under 365 nm excitation, in which only one broad emission band with peak at 545 nm is observed. The broad emission band originates from the $^3\text{P}_1 \rightarrow ^1\text{S}_0$ transition of Bi^{3+} .^{28,29} The emission intensity increases with Bi^{3+} concentration from $s = 0$ to $s = 0.050$, and no concentration quenching is observed. The inset in Figure 3 presents the variation of the relative height of the Bi^{3+} emission peaks at 545 nm with Bi^{3+} concentrations, where the height of the $(\text{Y}_{0.95}\text{Bi}_{0.05})\text{VO}_4$ sample at 545 nm is set as 100%. First, the increase of Bi^{3+} luminescence at $s = 0$ to 0.015 is determined to be rapid, then becomes slow at $s = 0.015$ to 0.025, and finally the increase remains stable with low speed at $s = 0.025$ to 0.050. A reasonable explanation for this phenomenon is that when the concentration of Bi^{3+} is far below its critical concentration, the intensity of Bi^{3+} emission will increase quickly as the Bi^{3+} concentration increases, and then remains stable when the concentration of Bi^{3+} is close to its critical concentration. Once the concentration of Bi^{3+} is higher than its critical concentration, the intensity of Bi^{3+} emission will decrease for the energy transfer among different Bi^{3+} ions.

Figure 4 displays the emission spectra of the samples in the second row with $t = 0.005$ and $s = 0–0.050$ in the combinatorial library under 365 nm excitation. The emission

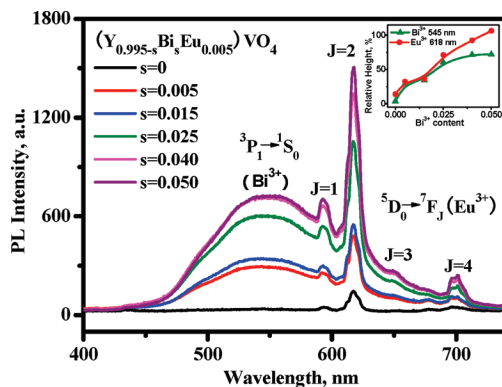


Figure 4. Emission spectra of the samples with $s = 0–0.050$ and $t = 0.005$ in the $(\text{Y}_{1-s-t}\text{Bi}_s\text{Eu}_t)\text{VO}_4$ combinatorial library under 365 nm excitation.

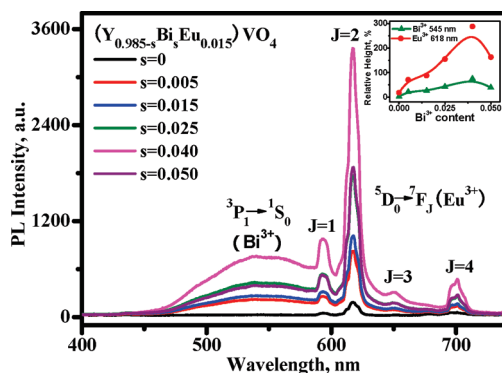


Figure 5. Emission spectra of samples with $s = 0–0.050$ and $t = 0.015$ in the $(\text{Y}_{1-s-t}\text{Bi}_s\text{Eu}_t)\text{VO}_4$ combinatorial library under 365 nm excitation.

lines at 592, 618, 650, and 702 nm are attributed to the $^5\text{D}_0 \rightarrow ^7\text{F}_J$ ($J = 1, 2, 3, 4$) transitions of Eu^{3+} and the broad emission band with a peak at 545 nm is assigned to the $^3\text{P}_1 \rightarrow ^1\text{S}_0$ transition of Bi^{3+} .^{28–30} The emission of Eu^{3+} still increases with Bi^{3+} concentration from $s = 0$ to $s = 0.050$, indicating that Bi^{3+} provides energy for Eu^{3+} to emit light. Meanwhile, the emission of Bi^{3+} also increases with Bi^{3+} concentration from $s = 0$ to $s = 0.040$. Unlike in Figure 3, there is no obvious increase in intensity of Bi^{3+} emission with concentration from $s = 0.040$ to $s = 0.050$, even though no significant decreases is observed. The inset of Figure 4 shows the variation of the relative height of the Eu^{3+} emission peaks at 618 nm and the Bi^{3+} emission peaks at 545 nm with Bi^{3+} concentrations: the increase in Eu^{3+} and Bi^{3+} emissions are similar to each other at $s = 0$ to 0.025, but the rate of increase of Eu^{3+} emission exceeds that of Bi^{3+} at $s = 0.025$ to 0.050, and there is almost no increase with $s = 0.040$ to 0.050 for the height of the Bi^{3+} emission peak. Therefore, the energy transfer from Bi^{3+} to Eu^{3+} does not influence Bi^{3+} emission if the concentration of Bi^{3+} is no higher than $s = 0.040$ and that of Eu^{3+} is less than $t = 0.005$; however, as Bi^{3+} concentration further increases to $s = 0.050$ and Eu^{3+} concentration is maintained at $t = 0.005$, the mean distance of Bi^{3+} and Eu^{3+} will be shortened, and then Eu^{3+} can capture energy from Bi^{3+} efficiently. Accordingly, Bi^{3+} emission is degraded evidently. Figure 5 shows this phenomenon more clearly.

Figure 5 presents the emission spectra of the samples in the third row with $t = 0.015$ and $s = 0–0.050$ in combina-

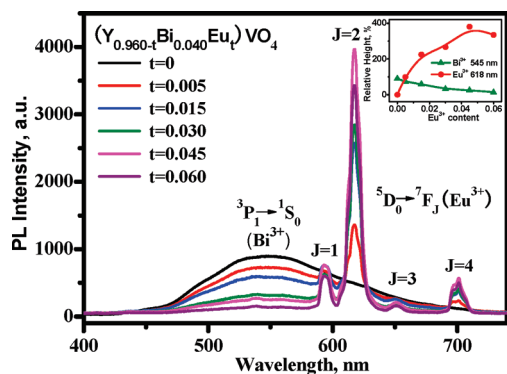


Figure 6. Emission spectra of samples with $s = 0.040$ and $t = 0–0.060$ in the $(Y_{1-s-t}Bi_sEu_t)VO_4$ combinatorial library under 365 nm excitation.

torial library under 365 nm excitation: the concentration of Bi^{3+} equals that in Figure 3 and Figure 4 with $s = 0–0.050$, but Eu^{3+} concentration is increased to $t = 0.015$. Figure 5 clearly shows that both Bi^{3+} and Eu^{3+} emissions increase with Bi^{3+} concentration from $s = 0$ to $s = 0.040$, but they decrease significantly as Bi^{3+} concentration increases from $s = 0.040$ to $s = 0.050$. Excessive Eu^{3+} co-doping has quenched the luminescence of Bi^{3+} and itself seriously. The inset in Figure 5 reveals that the Eu^{3+} and Bi^{3+} emissions are greatest at $s = 0.040$. Comparing Figures 3, 4, and 5, and in particular the relative height of Bi^{3+} emission peaks at 545 nm and Eu^{3+} emission peak at 618 nm presented as insets, demonstrates that the Bi^{3+} emission is strongest at $s = 0.050$ in Figure 3 and 4, but $s = 0.040$ in Figure 5; the Eu^{3+} emission is strongest at $s = 0.050$ in Figure 4, but $s = 0.040$ in Figure 5. These results demonstrate that the transfer of energy from Bi^{3+} to Eu^{3+} depends on the Bi^{3+} and Eu^{3+} interionic distance. This characteristic is typical of resonance energy transfer.

Figure 6 presents the emission spectra of the samples in the fifth column with $s = 0.040$ and $t = 0–0.060$ in the combinatorial library under 365 nm excitation: the emission of Bi^{3+} declines gradually as Eu^{3+} content increases from $t = 0$ to $t = 0.060$, further indicating that the transfer of energy from Bi^{3+} to Eu^{3+} to an extent that increases gradually with Eu^{3+} concentration, because of the shortening of the distance between Bi^{3+} and Eu^{3+} . However, the emission of Eu^{3+} increases with Eu^{3+} concentration from $t = 0$ to $t = 0.045$ and then declines as the Eu^{3+} concentration further increases from $t = 0.045$ to $t = 0.060$. This finding is clearly revealed by the variation of the relative height of Bi^{3+} and Eu^{3+} emission peaks presented in the inset in Figure 6. This phenomenon is well-known as concentration quenching of luminescence.

The emission spectra of other samples are omitted here. However, the relative luminescence efficiency of every sample in the combinatorial library obtained by integrating the emission spectrum from 400 to 700 nm is shown in Figure 7, from which the composition range of samples that displays relatively more efficient luminescence is $0.040 \leq s \leq 0.050$ and $0 < t \leq 0.015$ for $(Y_{1-s-t}Bi_sEu_t)VO_4$.

Besides efficiency, another factor that determines whether phosphors can be applied in LEDs is color quality. The color coordination (CIE(x,y)), correlated color temperature (Tc),

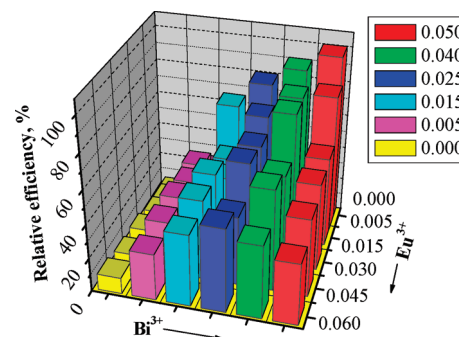


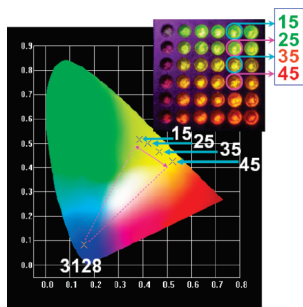
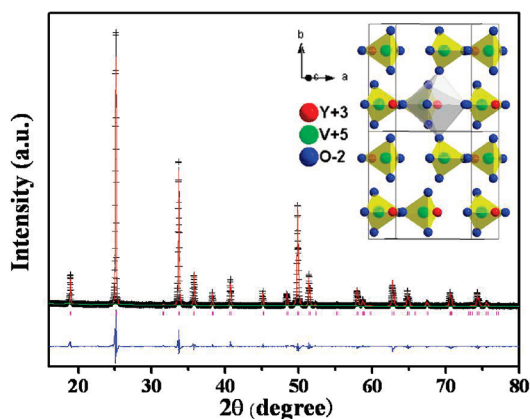
Figure 7. Relative emission efficiency of every sample in the $(Y_{1-s-t}Bi_sEu_t)VO_4$ combinatorial library determined by integration emission spectra from 400 to 700 nm under 365 nm excitation.

and color rendering index (Ra) of emission spectra, as corresponding to Figure 6, of the $(Y_{1-s-t}Bi_sEu_t)VO_4$ ($s = 0.040$; $t = 0–0.045$) samples obtained by calculating with the CIE13 software, are summarized in Table 1. The correlated color temperature decreases gradually from 4530 to 1781 K as Eu^{3+} concentration increases from $t = 0$ to $t = 0.045$, indicating that co-doping Eu^{3+} benefits to obtain warm light. The color rendering index increases with Eu^{3+} concentration from $t = 0$ to $t = 0.015$ and then decreases as Eu^{3+} increases from $t = 0.015$ to 0.045. This suggests that co-doping a little Eu^{3+} is helpful to improve color rendering; however, too much can be harmful. Figure 8 displays the CIE coordinates varying with Eu^{3+} concentration from $t = 0$ to $t = 0.030$ visually, where the color changes from yellow-green to orange. Differentiating from judging by visual inspection, the CIE diagram demonstrates the variation of emission color objectively without visual function effect. The highest Ra of 86.86 is obtained for the sample of $(Y_{0.945}Bi_{0.040}Eu_{0.015})VO_4$, which has been higher than that of YAG-based LEDs but lower than the value of 90–100 for the classified 1A grade Ra. However, there is no blue component in the emission spectrum of $(Y_{0.945}Bi_{0.040}Eu_{0.015})VO_4$. Otherwise, the Ra value would be higher. Figure 8 also presents the CIE coordinates of commercially available blue phosphor for NUV WLEDs, such as (0.1576, 0.0836) for $Sr_3MgSi_2O_8:Eu^{2+}$ (3128). On the basis of the principle that white light can be produced by mixing polychromatic lights, we make sure that an ideal WLED with high Ra can be tuned up by coating the optimized yellow phosphor and other blue phosphor onto a NUV diode chip within the CIE range of $0.3857 \leq x \leq 0.5224$ and $0.4250 \leq y \leq 0.5146$, as the triangle marked in Figure 8.

Conventional Experiments Results. To confirm the feasibility of the above results studied by combinatorial chemistry approach, some bulk samples were synthesized with the conventional solid state reaction method from sources of Y_2O_3 (99.9%), NH_4VO_3 (98%), $Eu(NO_3)_3 \cdot 5H_2O$ (99.99%), and Bi_2O_3 (99.5%). The same sintering technique as was employed in combinatorial library synthesis was used. Before sintering, the raw materials in a stoichiometric ratio were thoroughly ground. The photoluminescence (PL) of the bulk samples was measured using FluoroMax-3 and FluoroMax-p spectrometers. Thermal quenching luminescence was obtained by using a heating apparatus (THMS-600) and in combination with the spectrometer. The crystal structure

Table 1. Color Coordination (CIE(x,y)), Correlated Color Temperature (Tc), and Color Rendering Index (Ra) of Emission Spectra of the $(\text{Y}_{1-s-t}\text{Bi}_s\text{Eu}_t)\text{VO}_4$ ($s = 0.040$; $t = 0-0.030$) Samples in Combinatorial Library under 365 nm Excitation, As Corresponding to Figure 6

properties	samples									
	$(\text{Y}_{0.960}\text{Bi}_{0.040})\text{VO}_4$ (15)		$(\text{Y}_{0.955}\text{Bi}_{0.040}\text{Eu}_{0.005})\text{VO}_4$ (25)		$(\text{Y}_{0.945}\text{Bi}_{0.040}\text{Eu}_{0.015})\text{VO}_4$ (35)		$(\text{Y}_{0.930}\text{Bi}_{0.040}\text{Eu}_{0.030})\text{VO}_4$ (45)		$(\text{Y}_{0.915}\text{Bi}_{0.040}\text{Eu}_{0.045})\text{VO}_4$ (55)	
	x	y	x	y	x	y	x	y	x	y
color coordination (CIE(x,y))	0.3857	0.5146	0.4209	0.5003	0.4666	0.4651	0.5224	0.4250	0.5331	0.3853
correlated color temperature (Tc)	4530		3887		2999		2109		1781	
color rendering index (Ra)	56.98		68.35		86.86		82.04		71.63	

**Figure 8.** CIE coordinates of emission spectra of $(\text{Y}_{0.960}\text{Bi}_{0.040})\text{VO}_4$ (15), $(\text{Y}_{0.955}\text{Bi}_{0.040}\text{Eu}_{0.005})\text{VO}_4$ (25), $(\text{Y}_{0.945}\text{Bi}_{0.040}\text{Eu}_{0.015})\text{VO}_4$ (35), $(\text{Y}_{0.930}\text{Bi}_{0.040}\text{Eu}_{0.030})\text{VO}_4$ (45), and commercially available $\text{Sr}_3\text{MgSi}_2\text{O}_8:\text{Eu}^{2+}$ (3128) phosphors under 365 nm excitation.**Figure 9.** Experimental (crosses), calculated (solid line), and difference (bottom) results of XRD refinement of $(\text{Y}_{0.955}\text{Bi}_{0.040}\text{Eu}_{0.005})\text{VO}_4$. Inset presents the three-dimensional structure.

of bulk samples was identified by X-ray diffraction (XRD) analysis using an X'Pert PRO advanced automatic diffractometer with $\text{Cu K}\alpha$ radiation, operated at 45 kV and 40 mA. The GSAS program³¹ was used to perform the Rietveld refinements to obtain information on the crystal structure of $\text{YVO}_4:\text{Bi}^{3+},\text{Eu}^{3+}$.

YVO_4 has the well-known zircon type of crystal structure. The experimental, calculated, and difference results of the XRD refinement of $(\text{Y}_{0.955}\text{Bi}_{0.040}\text{Eu}_{0.005})\text{VO}_4$ at room temperature, obtained by using the GSAS program, are displayed in Figure 9.³¹ Table 2 presents the corresponding crystallographic data. $(\text{Y}_{0.955}\text{Bi}_{0.040}\text{Eu}_{0.005})\text{VO}_4$ crystallizes as a tetragonal structure (inset in Figure 9) with a space group of $I4_1/amd$ (141) and lattice constants of $a = b = 7.129(6)$ Å, $c = 6.301(6)$ Å, and v (cell volume) = $320.318(7)$ Å³. All of the observed peaks satisfy the reflection condition with

Table 2. Crystallographic Data for $(\text{Y}_{0.955}\text{Bi}_{0.040}\text{Eu}_{0.005})\text{VO}_4$

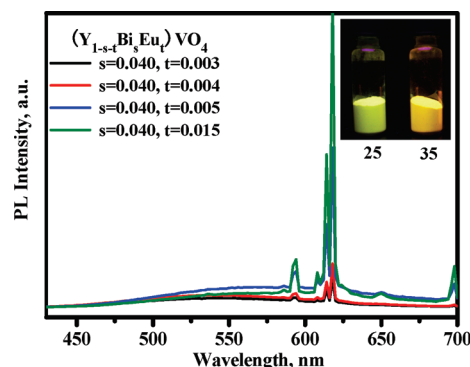
atoms	X	Y	Z	fraction	$U_i(\text{Å}^2)$
Y	0.0000(0)	0.750(0)	0.125(0)	0.955	0.0148(8)
V	0.0000(0)	0.250(0)	0.375(0)	1.000	0.0137(7)
O	0.0000(0)	0.433(3)	0.202(4)	1.000	0.0069(1)
Eu	0.0000(0)	0.750(0)	0.125(0)	0.005	0.0148(8)
Bi	0.0000(0)	0.750(0)	0.125(0)	0.040	0.0149(4)

Space Group: $I4_1/amd$

cell parameter	reliability factors
$a = b = 7.129(6)$ Å,	$\chi^2 = 1.569$
$c = 6.301(6)$ Å	Rwp = 5.17%
$\alpha = \beta = \gamma = 90^\circ$	Rp = 3.21%
cell volume = $320.318(7)$ Å ³	

reliability factors as follows: $\chi^2 = 1.569$, Rp = 5.17%, and Rwp = 3.21%. The cell volume is a little higher than that of the ideal YVO_4 (JCPDS card 16-0250, whose lattice constants are $a = b = 7.123$ Å, $c = 6.291$ Å, and $v = 319.19$ (Å³) crystal lattice, because the radii of free Bi^{3+} and Eu^{3+} are larger than that of Y^{3+} (Bi^{3+} :0.96, Eu^{3+} :0.95, and Y^{3+} :0.89). Accordingly, Bi^{3+} and Eu^{3+} should replace the ideal sites of Y^{3+} .

Figure 10 presents the emission spectra of $(\text{Y}_{0.957}\text{Bi}_{0.040}\text{Eu}_{0.003})\text{VO}_4$, $(\text{Y}_{0.956}\text{Bi}_{0.040}\text{Eu}_{0.004})\text{VO}_4$, $(\text{Y}_{0.955}\text{Bi}_{0.040}\text{Eu}_{0.005})\text{VO}_4$ (25), and $(\text{Y}_{0.945}\text{Bi}_{0.040}\text{Eu}_{0.015})\text{VO}_4$ (35) bulk samples under 365 nm excitation. For samples 25 and 35, Figure 10 clearly reveals that the emission intensity of Eu^{3+} increases and the Bi^{3+} emission declines as the Eu^{3+} concentration increases from $s = 0.005$ to $s = 0.015$. This result is consistent with the investigations cited above that utilized a combinatorial chemistry approach. The inset in Figure 10 shows the photograph of luminescence from samples 25 and 35 under 365 nm excitation. The colors are consistent with

**Figure 10.** Emission spectra of $(\text{Y}_{0.957}\text{Bi}_{0.040}\text{Eu}_{0.003})\text{VO}_4$, $(\text{Y}_{0.956}\text{Bi}_{0.040}\text{Eu}_{0.004})\text{VO}_4$, $(\text{Y}_{0.955}\text{Bi}_{0.040}\text{Eu}_{0.005})\text{VO}_4$ (25), and $(\text{Y}_{0.945}\text{Bi}_{0.040}\text{Eu}_{0.015})\text{VO}_4$ (35) under 365 nm.

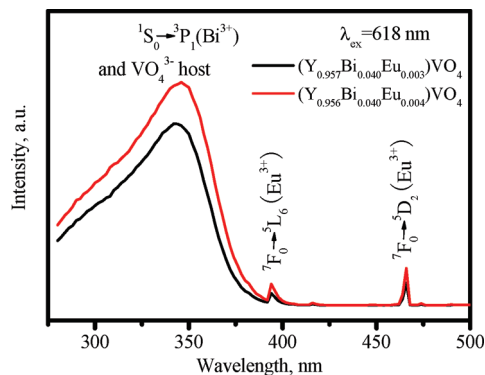


Figure 11. Excitation spectra of $(Y_{0.957}Bi_{0.040}Eu_{0.003})VO_4$ and $(Y_{0.956}Bi_{0.040}Eu_{0.004})VO_4$ upon Eu^{3+} emission at 618 nm.

those in the combinatorial library, as judged by visual inspection. Another very interesting finding is that both Bi^{3+} and Eu^{3+} emission intensities increase with Eu^{3+} content from $t = 0.003$ to $t = 0.004$ and then to $t = 0.005$. This result demonstrates that doping the proper amount of Eu^{3+} into $YVO_4:Bi^{3+}$ improves its green luminescence efficiency. At the same time, the necessary red component required for high-Ra white light is also obtained. Therefore, this method is a perfect means of obtaining high-Ra white light, both efficiency and color rendering index Ra were all improved.

Figure 11 presents the normalized excitation spectra of the bulk samples of $(Y_{0.957}Bi_{0.040}Eu_{0.003})VO_4$ and $(Y_{0.956}Bi_{0.040}Eu_{0.004})VO_4$ upon Eu^{3+} emission at 618 nm. This broad excitation band with a peak at 341 nm is attributed to the $^1A_1 \rightarrow ^1T_1$ transition of VO_4^{3-} and the $^1S_0 \rightarrow ^3P_1$ transition of Bi^{3+} , as discussed in the following paragraph. The absorption lines at 394 and 466 nm are attributed to the $^7F_0 \rightarrow ^5L_6$ and $^7F_0 \rightarrow ^5D_2$ transitions of Eu^{3+} . The presence of VO_4^{3-} and Bi^{3+} absorption in Eu^{3+} excitation spectra indicates that the transfer of energy from VO_4^{3-} to Eu^{3+} and Bi^{3+} to Eu^{3+} occurs simultaneously;³⁰ however, the $Bi^{3+} \rightarrow Eu^{3+}$ energy transfer is more efficient under 365 nm excitation because the YVO_4 host cannot absorb the energy of 365 nm excitation efficiently, which can be concluded from the significant difference of the luminescence of the combinatorial library between under 365 and 254 nm excitation. Here, both the absorption band in the region 250–385 nm and the absorption lines of the $^7F_0 \rightarrow ^5L_6$ and $^7F_0 \rightarrow ^5D_2$ transitions of Eu^{3+} increase with Eu^{3+} concentration from $s = 0.003$ to $s = 0.004$, further confirming that doping proper amount of Eu^{3+} into $YVO_4:Bi^{3+}$ increases its luminescence efficiency.

Finally, a practical white LED lamp has been prepared from an optimal $(Y_{0.956}Bi_{0.040}Eu_{0.004})VO_4$ phosphor and a commercially available blue phosphor of $Sr_3MgSi_2O_8:Eu^{2+}$ (3128) assisted by Everlight Electronics Co. Ltd. Figure 12 presents the emission spectrum of the prepared LED lamp, with a Ra of up to 90.3. The inset also presents the photographs of $(Y_{0.956}Bi_{0.040}Eu_{0.004})VO_4$ and 3128 phosphors luminescence taken under 365 nm excitation.

Mechanism of Luminescence and Theoretical Analysis.

To study the mechanism of luminescence and the paths of energy transfer during luminescence, the PL spectra of the YVO_4 pure host and the Bi^{3+} -doped YVO_4 bulk samples were examined and shown in Figure 13 (a) and (b),

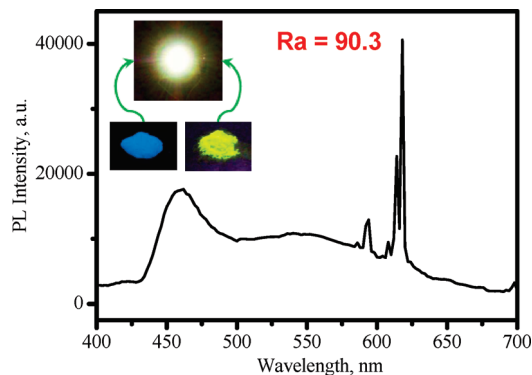


Figure 12. Emission spectrum of a warm-white LED lamp, fabricated by coating a NUV LED chip with commercially available $Sr_3MgSi_2O_8:Eu^{2+}$ (3128) and self-optimized $(Y_{0.956}Bi_{0.040}Eu_{0.004})VO_4$ phosphors.

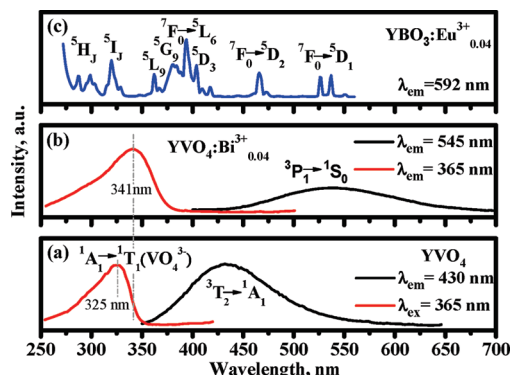


Figure 13. Emission and excitation spectra overlap of YVO_4 (a), $YVO_4:Bi^{3+}$ (b), and $YBO_3:Eu^{3+}$ (c).

respectively. The full energy level of Eu^{3+} ranged from 250 to 560 nm was obtained by measuring in the YBO_3 host, as shown in Figure 13 (c). The reason for selecting YBO_3 as host is that the absorption band of YBO_3 (150–175 nm) is far higher than the $O^{2-}-Eu^{3+}$ charge transfer (223 nm). Although no Bi^{3+} and Eu^{3+} were doped into YVO_4 , a strong emission band with a peak at around 430 nm was observed under 365 nm excitation, and a strong excitation band that peaked at approximately 325 nm was observed by monitoring 430 nm emission. These bands are attributed to charge transfer between the p^6 orbital of O^{2-} and the d orbital of V^{5+} within the polyanion of VO_4^{3-} . The ground state of VO_4^{3-} with the p^6 configuration is 1S_0 ($t_1^6, ^1A_1$), and the excited states that arise from $p^5d(t_1^5e)$ configuration with T_d space group and split by the crystal field are $^3T_2, ^3T_1, ^1T_1$, and 1T_2 in order of increasing energy, as shown in Figure 14(a).³² Therefore, the excitation band of YVO_4 in Figure 13 (a) is assigned to the spin allowed $^1A_1 \rightarrow ^1T_1$ transition of VO_4^{3-} . The electrons that occupy the 1T_1 excited state are unstable and tend to relax to the low 3T_2 or 3T_1 level. When an electron returns from an excited state to the ground state, a photon is emitted. Here, the emission-band peaked at about 430 nm is attributed to the $^3T_2 \rightarrow ^1A_1$ transition for $\Delta J = 1$ (where J represents the total angular momentum of the electron). Hence, the excitation and emission processes in YVO_4 can be summarized as Figure 14 (a).

The ground state of a free Bi^{3+} with ns^2 configuration is 1S_0 , and the excited states that arise from the $nsnp$ configuration are $^3P_0, ^3P_1, ^3P_2$, and 1P_1 in order of increasing

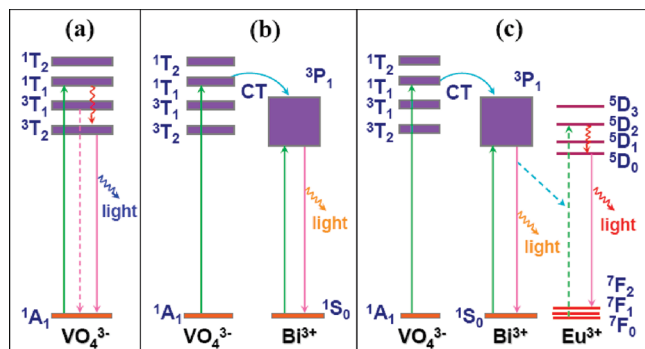


Figure 14. Schematic diagram of VO₄³⁻, Bi³⁺, and Eu³⁺ energy levels and excitation, emission, and energy transfer in YVO₄ (a), YVO₄:Bi³⁺ (b), and YVO₄:Bi³⁺,Eu³⁺ (c).

energy.^{33–35} Although the electron transition from *ns* to *nsnp* is allowed by the parity selection rule, by the spin selection rule, only the transition from ¹S₀ (or ¹P₁) to ¹P₁ (or ¹S₀) is allowed for $\Delta S = 0$ (where *S* denotes the spin angular momentum of the electron) if no other configuration is considered. However, the ¹S₀→³P₁ transition is made partially allowed by the mixing of the singlet state and the triplet state. Therefore, the emission band with a peak at 545 nm in Figure 13 (b) is attributed to ³P₁→¹S₀. A comparison with Figure 13 (a) reveals that the emission of ³T₂→¹A₁ transition of VO₄³⁻ is absent in the emission spectrum of YVO₄:Bi³⁺ under the same excitation condition. A reasonable explanation is that the absorption energy of VO₄³⁻ has been transferred to Bi³⁺. However, an extra absorption band over YVO₄ excitation occurs to the excitation spectrum of YVO₄:Bi³⁺, as shown in Figure 13 (b). Datta²¹ attributed this extra band to O–V and O–Bi charge transfer. The transfer of charge from O²⁻ of VO₄³⁻ to Bi³⁺ properly explains the transfer of energy from VO₄³⁻ to Bi³⁺, but the significant difference of luminescence of the above combinatorial library between under 365 nm and under 254 nm excitation indicates electrons are directly excited from the ¹S₀ ground state to the ¹P₁ excited state when exciting with low energy 365 nm. If excited with 254 nm, electrons are mainly excited from the ¹A₁ ground state to the ¹T₁ excited state of VO₄³⁻. Hence, the excitation band in the region 250–385 nm in Figure 13 (b) is attributed to the common contribution of the host sensitization band from VO₄³⁻ to Bi³⁺ via O²⁻–Bi³⁺ charge transfer and the ¹S₀→³P₁ transition of Bi³⁺. Accordingly, the excitation and emission processes of YVO₄:Bi³⁺ luminescence can be summarized as in Figure 14 (b).

The concentration dependence of Eu³⁺ luminescence, described above, demonstrates that the transfer of energy from Bi³⁺/VO₄³⁻ to Eu³⁺ is by resonance. The resonant energy levels between the emission of the sensitizer and the absorption of the activator must match well to satisfy the critical requirement of an efficient energy transfer, and the probability of energy transfer between the sensitizer and the activator is expressed, according to Dexter,³⁶ as

$$P_{SA} = \frac{2\pi}{h} |\langle SA^* | H_{SA} | S^* A \rangle|^2 \int g_s(E) g_A(E) dE \quad (1)$$

where the matrix represents the interaction between the initial state $|S^*A\rangle$ and final state $\langle SA^*|$, H_{SA} is the interaction

Hamiltonian, *S* and *A* represent the emitter and the absorber, $g_s(E)$ and $g_A(E)$ are normalized optical line shape functions, and the integral represents the spectral overlap, respectively. The ³P₁→¹S₀ emission of Bi³⁺ largely overlaps the ⁷F₀→⁵D₂ and ⁷F₀→⁵D₁ excitation of Eu³⁺, as shown in Figures 13 (b) and (c). Accordingly, Bi³⁺ can efficiently transfer its absorption energy to Eu³⁺. However, the probability of energy transfer P_{SA} is proportional to $(1)/(R^6)$ (where *R* represents the distance between the sensitizer and the activator). If the distance between the sensitizer and the activator is too long, then excitation energy cannot be transferred to activators. Thus, strong emission of Bi³⁺ is observed when the Eu³⁺ concentration is very low; and almost no Bi³⁺ emission occurs when the Eu³⁺ concentration is very high, as presented in Figures 4, 5, 6, and 10. Therefore, the energy transfer in YVO₄:Bi³⁺,Eu³⁺ can be summarized as in Figure 14 (c).

Additionally, the ³T₂→¹A₁ emission of VO₄³⁻ largely overlaps the ⁷F₀→⁵L₉, ⁵G₉, ⁵L₆, ⁵D₃, and ⁵D₂ excitation of Eu³⁺, as displayed in Figures 13 (a) and (c), but YVO₄ exhibits almost no absorption when it is excited by 365 nm, as shown in Figure 13 (a). This fact explains the significant difference between Figure 1 and Figure 2 described above.

The above combinatorial research results reveal that $s = 0.040$ and $t = 0.005$ is approximately the critical concentration for the transfer of energy between Bi³⁺ and Eu³⁺ in the (Y_{1-s-t}Bi_sEu_t)VO₄ crystal lattice. Accordingly, the mean critical distance between Bi³⁺ and Eu³⁺ ions for energy transfer can be estimated using the relation that was proposed by Blasse and Grabmaier,³⁷

$$R_c \approx 2 \left(\frac{3V}{4\pi\chi_c Z} \right)^{1/3} \quad (2)$$

where *V* is the volume of the unit cell, χ_c is the sum of the critical concentration of the activator and the sensitizer, and *Z* is the number of formula units per unit cell. For (Y_{0.955}Bi_{0.040}Eu_{0.005})VO₄ phosphor, $V = 320.3158 \text{ \AA}^3$, $\chi_c = 0.045$, $Z = 4$. Therefore, the obtained R_c value is 15.0375 Å. A larger R_c value corresponds to a more efficient energy transfer.

Conclusions

Instead of developing a novel red phosphor individually, this work proposes the production of white light by combining a near-ultraviolet/ultraviolet diode chip with a blue and a red-green dual color phosphor so as to improve the color rendering of white light-emitting diodes. The possibility of this scheme was demonstrated, and the desired dual-color phosphor has been successfully screened out from the YVO₄:Bi³⁺,Eu³⁺ system using a combinatorial chemistry approach. When the emission color and luminous efficiency are both considered, the optimal composition is $0.040 \leq s \leq 0.050$ and $0 < t \leq 0.015$ for (Y_{1-s-t}Bi_sEu_t)VO₄. The red component that is required for a high-Ra WLED is obtained through the sensitizing luminescence of Eu³⁺ by Bi³⁺ in YVO₄ host; meanwhile, both Bi³⁺ and Eu³⁺ emission are improved by keeping the Bi³⁺ content close to the critical concentration. The transfers of energy from Bi³⁺ to Eu³⁺ and VO₄³⁻ to Eu³⁺ in the YVO₄ host are

through the resonance way; comparatively, $\text{Bi}^{3+} \rightarrow \text{Eu}^{3+}$ plays a more important role in transfer energy for Eu^{3+} to produce red light under NUV excitation.

Acknowledgment. The authors would like to thank the National Science, Taiwan, for financially supporting this research under Contract Nos. NSC 97-2113-M-002-012-MY3 and NSC 97-3114-M-002-005). The Postdoctoral Science Foundation of China (20090450802), the Postdoctoral Research Fellow of Materials Science and Engineering of Hefei University of Technology (103-035038) and the Science Foundation for Excellent Young Scholars of the Ministry of Education of China (20090111120001) also supported this research. Everlight Electronics Co. Ltd is commended for its assistance in preparing the LED lamps.

References and Notes

- (1) Neeraj, S.; Kijima, N.; Cheetham, A. K. *Chem. Phys. Lett.* **2004**, *387*, 2.
- (2) Nishida, T.; Ban, T.; Kobayashi, N. *Appl. Phys. Lett.* **2003**, *82*, 3817.
- (3) Kim, J. S.; Jeon, P. E.; Choi, J. C.; Park, H. L.; Mho, S. I.; Kim, G. C. *Appl. Phys. Lett.* **2004**, *84*, 2931.
- (4) Liu, R. S.; Liu, Y. H.; Bagkar, N. C.; Hu, S. F. *Appl. Phys. Lett.* **2007**, *91*, 061119.
- (5) <http://www.ledsmagazine.com/news/3/3/14>.
- (6) http://www.nichia.com/about_nichia/index.html.
- (7) <http://china.nikkeibp.com.cn/cgi-bin/cgi-bin/news/elec/6614-200805200123.html>.
- (8) Taniyasu, Y.; Kasu, M.; Makimoto, T. *Nature* **2006**, *441*, 325.
- (9) Sohn, K. S.; Park, D. H.; Cho, S. H.; Kim, B. I.; Woo, S. I. *J. Comb. Chem.* **2006**, *8*, 44.
- (10) Sohn, K. S.; Park, D. H.; S. H.; Cho, J. S.; Kwak, J. S.; Kim, *Chem. Mater.* **2006**, *18*, 1768.
- (11) Kulshreshtha, C.; Sharma, A. K.; Sohn, K. S. *J. Comb. Chem.* **2008**, *10*, 421.
- (12) Rodemerck, U.; Baerns, M.; Holena, M.; Wolf, D. *Appl. Surf. Sci.* **2004**, *223*, 168.
- (13) Schneider, G.; Wrede, P. *Prog. Biophys. Mol. Biol.* **1998**, *70*, 175.
- (14) Olender, R.; Rosenfeld, R. *J. Chem. Inf. Comput. Sci.* **2001**, *41*, 731.
- (15) Weber, L. *Curr. Opin. Chem. Biol.* **1998**, *2*, 381.
- (16) Gillet, V. J.; Khatib, W.; Willett, P.; Fleming, P. J.; Green, D. V. S. *J. Chem. Inf. Comput. Sci.* **2002**, *42*, 375.
- (17) Young, S. S.; Wang, M.; Gu, F. *J. Chem. Inf. Comput. Sci.* **2003**, *43*, 1916.
- (18) Xie, R. J.; Hirotsaki, N. *Sci. Technol. Adv. Mater.* **2007**, *8*, 588.
- (19) Kim, J. S.; Kwon, A. K.; Park, H. Y.; Choi, J. C.; Park, H. L.; Kim, G. C. *J. Lumin.* **2007**, *122–123*, 583.
- (20) Ma, L.; Wang, D.; Mao, Z.; Lu, Q.; Yuan, Z. *Appl. Phys. Lett.* **2008**, *93*, 144101.
- (21) Datta, R. K. *J. Electrochem. Soc.: Solid State Sci.* **1967**, *114* (10), 1057.
- (22) Park, W. J.; Jung, M. K.; Yoon, D. H. *Sens. Actuators, B* **2007**, *126*, 324.
- (23) Mahalley, B. N.; Dhoble, S. J.; Pode, R. B.; Alexander, G. *Appl. Phys. A: Mater. Sci. Process.* **2000**, *70*, 39.
- (24) Toma, S. Z.; Mikus, F. F.; Mathers, J. E. *J. Electrochem. Soc.: Solid State Sci.* **1967**, *114* (9), 953.
- (25) Neeraj, S.; Kijima, N.; Cheetham, A. K. *Solid State Commun.* **2004**, *131*, 65.
- (26) Chan, T. S.; Kang, C. C.; Liu, R. S.; Chen, L.; Liu, X. N.; Ding, J. J.; Bao, J.; Gao, C. *J. Comb. Chem.* **2007**, *9*, 343.
- (27) Chen, L.; Bao, J.; Gao, C.; Huang, S.; Liu, C.; Liu, W. *J. Comb. Chem.* **2004**, *6*, 699.
- (28) Chen, L.; Jiang, Y.; Zhang, G.; Wu, C.; Yang, G.; Wang, C.; Li, G. *Chin. Phys. Lett.* **2008**, *25* (5), 1884.
- (29) Chen, L.; Zheng, H.; Cheng, J.; Song, P. *J. Lumin.* **2008**, *128* (12), 2027.
- (30) Chen, L.; Yang, G.; Liu, J.; Shu, X.; Jiang, Y.; Zhang, G. *J. Appl. Phys.* **2009**, *105*, 013513.
- (31) Larson, A. C.; Von Dreele, R. B. *Generalized Structure Analysis System (GSAS)*; Los Alamos National Laboratory Report LAUR 86–748; Los Alamos National Laboratory: Los Alamos, NM, 1994.
- (32) Xu, X. R.; Su, M. Z. *Luminescence and Luminescent Materials*; Chemical Industry Press: Beijing, 2004; p 178.
- (33) Wang, M.; Fan, X.; Xiong, G. *J. Phys. Chem. Solids.* **1995**, *56*, 859.
- (34) Kim, C. H.; Park, H. L.; Mho, S. *Solid State Commun.* **1997**, *101* (2), 109.
- (35) Pode, R. B.; Dhoble, S. *Phys. Status Solidi B* **1997**, *203*, 571.
- (36) Blasse, G.; Grabmaier, B. C. *Luminescent Materials*; Springer-Verlag: Berlin, Heidelberg, 1994; p 92.
- (37) Blasse, G. *Philips Res. Rep.* **1969**, *24*, 131.

CC100063X